Scale-Up Manufacturing of PEG-Based Electrolytes for All-Solid-State Batteries Using Slot-Die Coating

Federico Reymundo Cardenas Zedano

A thesis

submitted in partial fulfillment of the

requirements for the degree of

Master of Science

University of Washington

2026

Committee:

Devin MacKenzie

Tucker Murray

Program Authorized to Offer Degree:

Materials Science and Engineering

University of Washington

Abstract

Scale-Up Manufacturing of PEG-Based Electrolytes for All-Solid-State Batteries Using Slot-Die Coating

Federico Reymundo Cardenas Zedano

Chair of the Supervisory Committee:

Devin MacKenzie

Department of Materials Science and Engineering

As demand for safer, higher-performance batteries continues to grow, scaling up all-solid-state battery manufacturing has become a critical challenge. Slot-die coating offers a promising first step toward continuous, roll-to-roll production of solid electrolytes. In this study, we demonstrate the feasibility of slot-die coating a poly(ethylene glycol) (PEG)-based photopolymer electrolyte to produce uniform, scalable films. The electrolyte formulation was adapted from compositions reported in the literature, while coating and curing conditions were optimized by integrating a UV lamp into the slot-die coater and systematically adjusting the curing distance. Silica nanoparticles concentration was varied from 4–12 wt.% to tune the rheological properties of the electrolyte and improve the coating quality. This approach produced homogeneous PEG-based electrolyte films directly on graphite electrodes. The coated electrolytes on electrodes were incorporated into coin cells and characterized using electrochemical impedance spectroscopy (EIS). The slot-die-coated electrolytes exhibited ionic conductivities on the order of 10^{-6} S cm^{-1}, comparable to values reported for polymer electrolytes in the literature (10^{-6} -10^{-4} S cm^{-1}). These results demonstrate the viability of slot-die coating as a scalable manufacturing method for PEG-based solid polymer electrolytes and establish an important foundation for their future roll-to-roll production.

Contents

List of Figures

List of Tables

Chapter 1: Introduction

1.1 Background

The battery industry is projected to grow 30% annually until 2030[1]. This growth is driven mainly by the increase in demand for battery electric vehicles (BEV), consumer electronics, and grid level storage[2]. This demand and growth projections have highlighted how important it is to be able to scale-up battery manufacturing for the future of electrification. However, scaling-up battery production can be difficult due to safety concerns, reliability, and manufacturability profitably at scale[3].

The main advantage of solid electrolyte batteries is the safety due to these kind of batteries not having a flammable liquid electrolyte inside them, thus the probability of fires during thermal runaway are greatly reduced[4]. The main issues with polymer electrolytes in specific is their lower ionic conductivities ($1 \times 10^{-6}\,\mathrm{S\,cm^{-1}}$ to $1 \times 10^{-4}\,\mathrm{S\,cm^{-1}}$) in comparison to other types of solid electrolytes at room temperature[5]. But, at higher temperatures polymer electrolytes can achieve much higher ionic conductivities ($> 1 \times 10^{-3}\,\mathrm{S\,cm^{-1}}$)[6, 7]. This can be used for grid level storage, which would help complement the large demand for liquid electrolyte batteries for other applications. Due to the nature of polymer solid electrolyte batteries, we could help reduce the safety reliability problem with large scale battery manufacturing. Another main issue with polymer electrolytes is the interfacial resistance due to not having perfect interfacial contact with the electrodes. Some advantages, other than safety, include good mechanical stability, easy processability compared to liquid electrolytes, better interfacial contact than other solid electrolytes, and they can be used for a wide range of applications that do not require high ionic conductivity or that can keep the battery at higher temperatures 60 °C to 100 °C[5, 4].

Poly(ethylene glycol)(PEG)-based electrolytes are great at dissociating lithium salts like LiTFSI into Li^+ and $TFSI^-$ components, this ability to dissociate lithium salts helps generating mobile Li^+ ions[8]. While this is beneficial for ionic conductivity some of the freed Li^+ ions will

bind to the PEG and hinder the ionic transport kinetics, which will lower the ionic conductivity[8, 9].

Explain the role of ether oxygen groups in lithium-ion coordination and transport.

1.2 Slot-Die Coating

Slot-die coating roll-to-roll manufacturing is the main way battery electrodes are manufactured nowadays[10], by using sheet-to-sheet slot-die coating as a first step we can eventually have an easier time scaling-up to roll-to-roll manufacturing without having to change our process as drastically as from small scale experiments to large area coatings. The need to scale-up manufacturing is a necessary step to be able to bring polymer electrolyte batteries to the market. By having a higher production of polymer electrolyte batteries we can achieve a more robust battery supply chain by not straining the liquid electrolyte production which is needed for other applications. By having a large volume of polymer electrolyte batteries we will be able to achieve a higher coverage of grid scale energy storage which will help with electrification of transportation and other areas of the economy which will help reduce the emission of greenhouse gases, making the grid more reliable and less suceptible to changes in fossil fuel prices[11]

1.3 Research Objectives

The objectives of this thesis are to recreate a PEG-based solid polymer electrolyte found in literature[12], then modifying it to be able to slot-die coat with it by changing the Aerosil 380 concentrations to modify the resin rheology. We will also be optimizing the chemistry, curing conditions, and coating parameters for the resin to produce a homogeneous polymer electrolyte film on graphite electrodes. We will then proceed to measure the ionic conductivity we achieve by making these large area films, and putting them in a half-cell coin cell device, from the ionic conductivity measurements and the film homogeneity we will conclude what the optimal conditions found are, and evaluate the future steps for larger scale manufacturing of our polymer electrolyte chemistry.

Chapter 2: Experimental Methods

2.1 Materials

For the polymer electrolyte, poly(ethylene glycol) methyl ether acrylate (PEGMEA; $M_n = 480\,\mathrm{g\,mol^{-1}}$, 100 ppm monomethyl ether hydroquinone (MEHQ) inhibitor, and 100 ppm butylated hydroxytoluene (BHT) inhibitor), poly(ethylene glycol) diacrylate (PEGDA; $M_n = 250\,\mathrm{g\,mol^{-1}}$, 100 ppm MEHQ inhibitor), phenylbis(2,4,6-trimethylbenzoyl)phosphine oxide (Irgacure 819; 97%, powder), 2,2-dimethoxy-2-phenylacetophenone (DMPA; 99%), lithium bis(trifluoromethanesulfonyl)imide (LiTFSI; 99.99%, trace-metals basis), and anhydrous sodium sulfate (≥ 99.0%) were supplied by Sigma-Aldrich. AEROSIL 380 silica, with a specific surface area of $380\,\mathrm{m^2\,g^{-1}}$, was supplied by Evonik.

For the electrode substrate, MesoCarbon MicroBeads (MCMB) graphite powder (99.96%), carbomethyl cellulose sodium salt (Na-CMC), super C65 conductive carbon, styrene-butadiene rubber 50wt% solution in water (SBR), and the 9 um thickness copper foil were supplied by MTI Corporation.

Table 1: Materials, suppliers, and application.

Material	Supplier	Function
PEGDA	Sigma-Aldrich	Crosslinking monomer
PEGMEA	Sigma-Aldrich	Crosslinking monomer
LiTFSI	Sigma-Aldrich	Lithium salt
Aerosil 380	Evonik	Inorganic filler
DMPA	Sigma-Aldrich	Photoinitiator
Irgacure 819	Sigma-Aldrich	Photoinitiator
Sodium sulfate	Sigma-Aldrich	Resin desiccant
MCMB graphite	MTI Corporation	Electrode active material
Na-CMC	MTI Corporation	Electrode binder
Conductive carbon	MTI Corporation	Electrode conductive additive
50% SBR solution	MTI Corporation	Electrode binder
Copper foil	MTI Corporation	Electrode current collector

2.2 Electrolyte Formulation

Electrolyte forumulation started by measuring 4-12wt% Aerosil 380 and placing it in a vacuum oven for 24 hours to remove any moisture. Then a 9:1 ratio of PEGMEA to PEGDA was measured in a fume hood, transferred into a nitrogen glovebox, and then 2wt% of sodium sulfate was added to the mixture as a dissecant and stirred in the glovebox for 2h. Then the solution was decanted to remove the sodium sulfate and trace moisture precipitants. Then 10wt% of LiTFSI was added and stirred for 12h. Then, the aerosil was transferred into the glovebox, and resin would be poured into a THINKY planetary mixing cup with 1/3 of the Aerosil, mixed for 30 seconds at 2000rpm, then added the aerosil in two more steps both mixed for 30 seconds at 2000 rpm. Then finally 0.01-1wt% of the photoinitiator (either DMPA or Irgacure 819) was added and thinky mixed for 1 minute at 2000 rpm. Finally the resin was put into a 60 mL syringe for slot-die coating.

2.3 Characterization

The rheological characterization was performed using an Anton Paar MCR 302 rheometer equipped with a 25 mm diameter, 2° cone–plate geometry CP25-2. Measurements were conducted at 20 °C over a shear-rate range of 0.01 s^{-1} to 100 s^{-1}. The film thicknesses were measured using a Dektak XTL stylus profiler equipped with a 0.2 µm tip and an applied force of 1 mg. Electrochemical impedance spectroscopy (EIS) measurements were performed using VersaSTAT 4 and PARSTAT 4000A potentiostat in EIS mode over a frequency range of 1–10^6 Hz, with an AC amplitude of 20 mV RMS at room temperature.

2.4 Slot-Die Coating

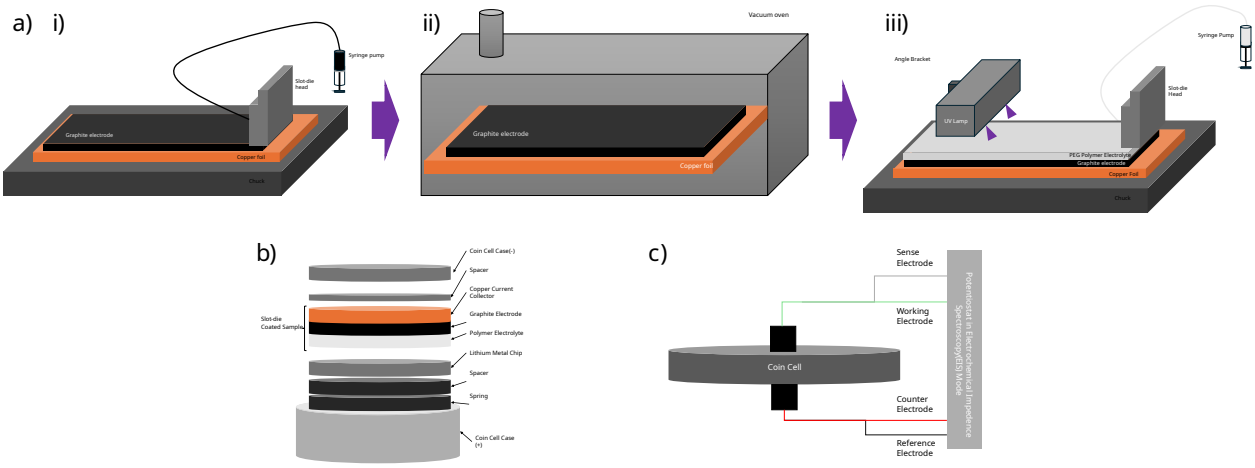

Figure 1: Process overview and testing for device stack. (a) Manufacturing overview, (i)slot-die coating of graphite electrode on the prepared copper foil. (ii)graphite electrode in vacuum oven to remove solvent. (iii) Slot-die coating of polymer electrolyte on graphite electrode and cured in-situ by UV lamp installed in FOM Alpha roll-to-roll slot-die coater using an angle bracket. (b) Device stack to test electrochemical performance of the slot-die coated samples (c) Electrochemical impedance spectroscopy two probe test set up.

All the slot-die coating was done using the FOM AlphaR2R. The slot-die coating started with a 50% solids loading 94.5wt% MCMB graphite, 2wt% CMC, 1.5wt% SBR, and 2wt% conductive carbon which was slot-die coated on a copper foil current collector which was cleaned using IPA and coated with the followng parameters (Figure 1ai): die head height of 100 µm, a 0.1 m min^{-1} coating speed, 188 µL min^{-1} pumprate, and 25 µm die length. This sample was then dried overnight at 90°C (Figure 1aii). This was then placed back on the slot-die coater and the electrolyte was coated using a wide range of coating conditions and cured while coating using a UV lamp installed into the AlphaR2R using an angle bracket (Figure1aiii).

2.5 Electrochemical Impedance Spectroscopy

For EIS our cell configuration consisted of: positive coin cell case, spring washer, 1mm stainless steel spacer, lithium metal chip, our slot-die coated polymer electrolyte on graphite electrode on copper current collector, a 0.2mm spacer and negative coin cell case built in an Ar gas glove box. The testing frequency range was 1 Hz to 1×10^6 Hz with an AC amplitude of 20 mV RMS, measured

at room temperature. The bulk resistance was found by using the end of the high frequency range parabola in the Nyquist plot Figure 5a

The ionic conductivity was calculated using[13]:

$$\sigma = \frac{h}{R_b A} \tag{2.1}$$

where σ is the ionic conductivity, h is the electrolyte thickness, R_b is the bulk resistance, and A is the electrolyte film area.

Chapter 3: Process Optimization

3.1 Experimental Design

We had six optimization parameter we decided to explore during this research Table 2: curing distance, curing time, Aerosil 380 concentration, coating speed, flow rate, and coating gap. We tested four sample per optimization parameter and from that we got our top performers, and we used those films to gather ex-situ data to quantify which one had the best performance. From our two best samples we made sample replicates.

Table 2: Optimization space.

Variable	Minimum	Maximum
UV-curing distance (cm)	7	70
UV-curing time (s)	5	600
Aerosil 380 concentration (wt%)	4	12
Coating speed ($\mathrm{m\,min^{-1}}$)	0.01	1
Flow rate ($\mu\mathrm{L\,min^{-1}}$)	200	1000
Coating height (μm)	50	150
Photoinitiator concentration (wt%)	0.01	1

3.2 UV Curing Optimization

a)

b)

c)

Figure 2: UV curing optimization experiment results showing ideal film and two different suboptima conditions, (a) overcured and uneven curing sample with 0.1wt% Irgacure 819 photoinitiator, (b) undercured sample with 0.1 wt% DMPA photoinitator, (c) optimized sample using 0.2 wt% DMPA, cured for 1 minute at 7 cm.

For our first optimization experiment, we blade coated samples and cured them using the UV lamp for different amounts of time, curing distance, photoinitator, and photoinitiator concentration. From this we could qualitatively tell if the sample was overcured (Figure2a), undercured (Figure2b), or if it was an acceptable film (Figure2c). From these experiments we determined that the Irgacure 819 was not a suitable photoinitiator, since it was overcuring or curing before we were able to use it due to the lights at the lab initiating the polymerization. We decided to use DMPA due to their peak absorption being deeper in the UV range, we also determined 0.2wt% DMPA was the best photoinitiator concentration, and the optimal curing conditions were curing for 1 minute at 7 cm.

3.3 Rheological Optimization

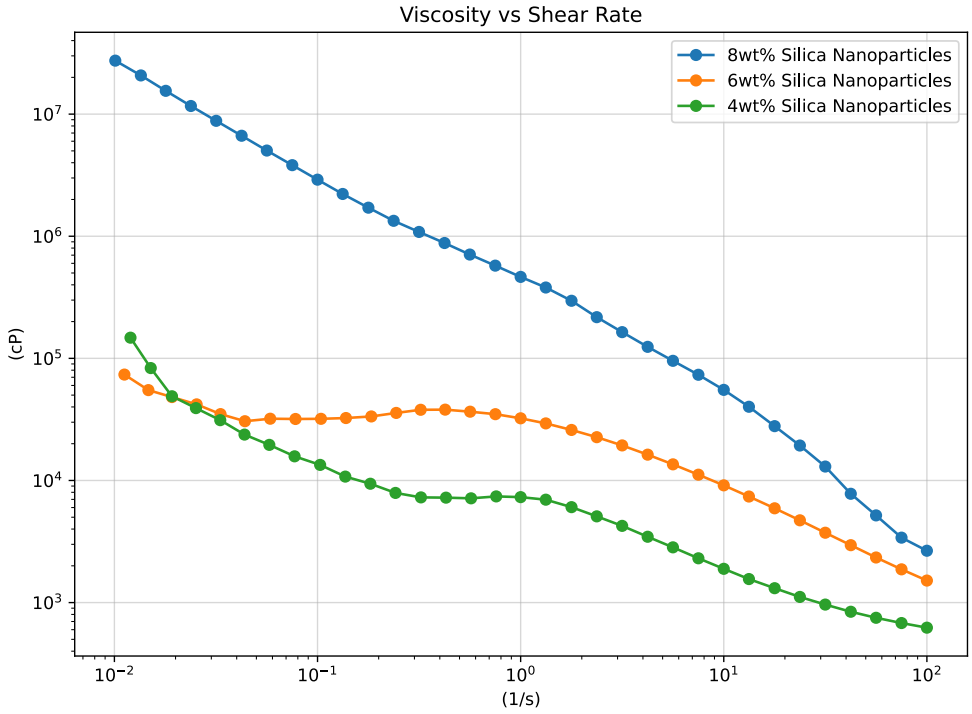

Figure 3: Rheological behaviour of uncured resin at shear rates of 0.01-100 s^{-1} with different Aerosil 380 concentrations (8-4wt%).

The concentration of Aerosil 380 was the main determining factor affecting resin rheology. We tested a range of Aerosil 380 concentrations of 4 wt% to 12 wt% Figure3. The 10wt% and

12wt% samples were too viscous to test using the rheometer available. The 8wt% sample was too viscous for slot-die coating using a plastic syringe. The 4wt% and 6wt% samples were suitable for slot-die coating, so we used them as a basis for the slot-die coating optimization.

3.4 Slot-Die Coating Optimization

For the slot-die coating optimization we used a wide range of coating parameters shown in Table 2. We changed the coating speed (0.01-1m min^{-1}), pump flow rate (200-1000 µL min^{-1}), and die head height (50-150 µm). From these parameters and the rheological data from Section 3.3, we optimized the coating parameters for both the 6wt% and 8wt% Aerosil concentration samples.

3.5 Optimized Conditions

From all the optimization steps we determined the optimized coating and curing conditions for our two best resin formulations for slot-die coating. For both samples we determined the ideal coating conditions to be a 0.1 m min^{-1} coating speed, 80 µm coating height, and a UV curing distance of 7 cm. With the only variable that changed between the two samples being the pump flow rate which was 375 µL min^{-1} for the 4wt% Aerosil 380 resin and 500 µL min^{-1} for the 6wt% Aerosil 380 resin (3). With these coating conditions for these formulations we were able to achieve a homogeneous film.

Table 3: Optimized coating conditions.

Parameter	4wt% Aerosil	6wt% Aerosil
Coating speed (m min^{-1})	0.1	0.1
Flow rate (µL min^{-1})	375	500
Coating height (µm)	80	80
UV curing distance (cm)	7	7

Chapter 4: Results and Discussion

4.1 Slot-Die Coating Performance

At first, we struggled to get homogeneous coats due to multiple issues between them, clogging, flooding, ribbing, and a large amount of entrapped air in the resin. As seen in Figure 4a we have an inhomogeneous slot-die coated sample on copper foil, which was caused by ribbing and clogging. We were able to achieve a relatively homogeneous coat in Figure 4b using the optimizations discussed in Section 3. Although the samples are relatively homogeneous, there is still room for improvement with further process optimizations to reduce surface roughness and edge quality. Another area for improvement would be to further reduce bubbles before coating.

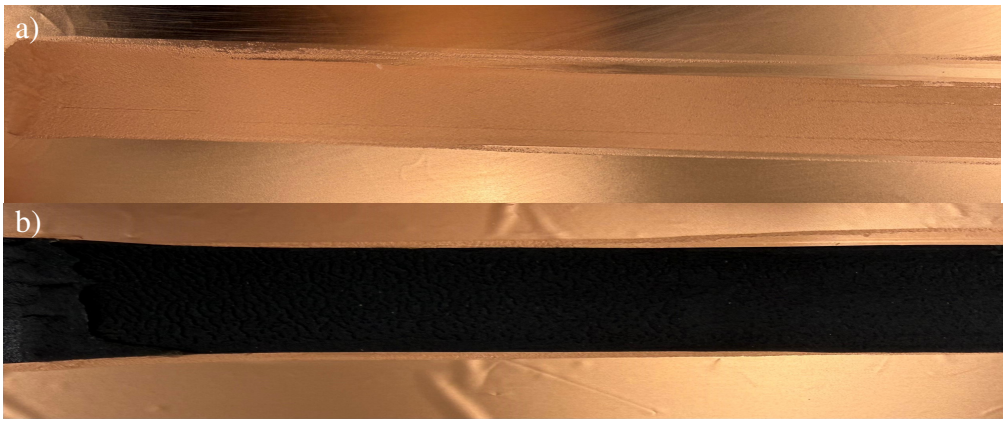

Figure 4: Images of slot-die coated polymer electrolyte samples, (a)inhomogeneous slot-die coated polymer electrolyte on copper foil, (b)homogeneous slot-die coated polymer electrolyte on graphite electrode

4.2 Electrochemical Impedance Spectroscopy and Ionic Conductivity

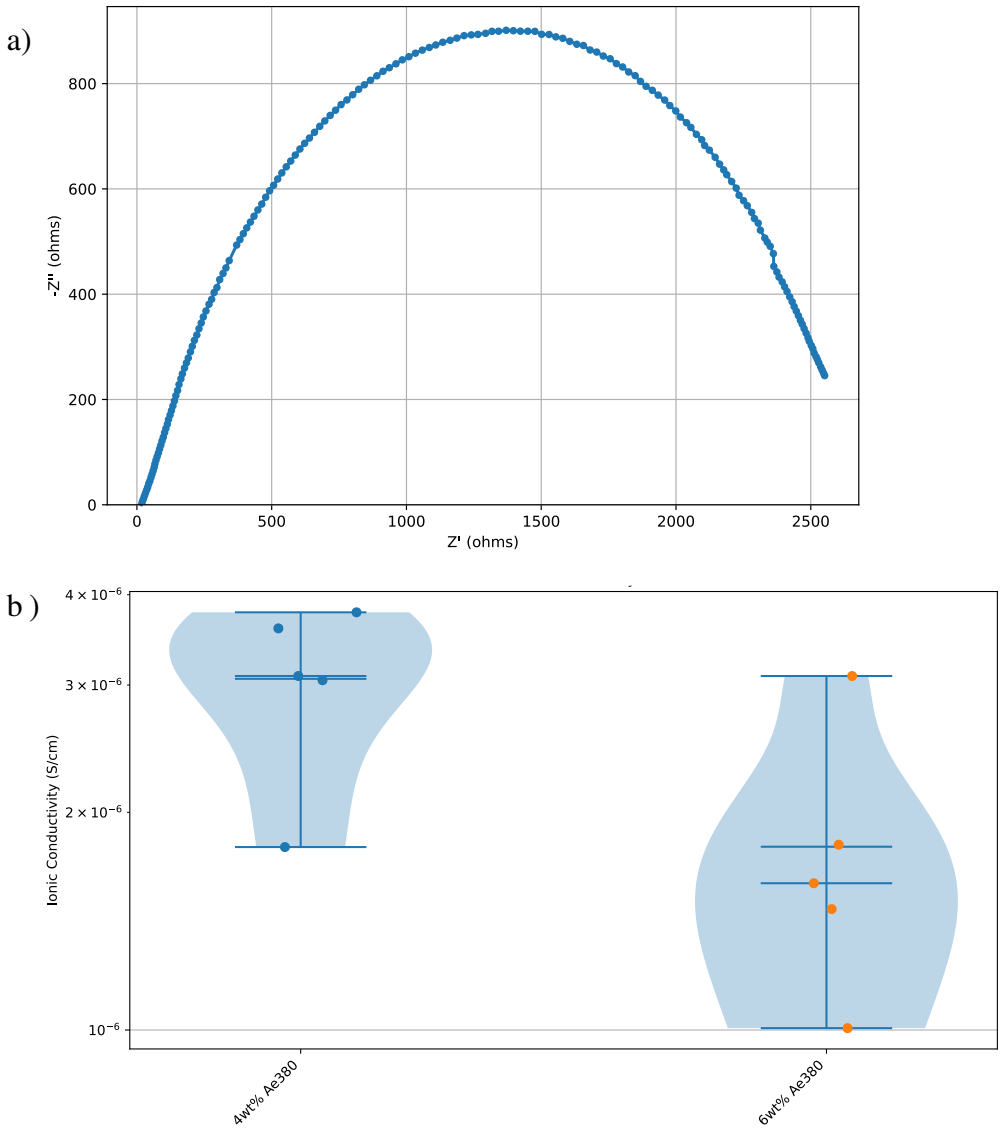

Figure 5: (a) Representative Nyquist plot at the high frequency semicircle of EIS test (10^4–10^6 Hz). (b) Ionic conductivity violin plot for all slot-die coated samples.

As mentioned in Section 2.5, the bulk resistance was determined from the high-frequency semicircle and then the ionic conductivity was calculated using Equation 2.1. We were able to achieve our highest ionic conductivities with the 4 wt.% Aerosil 380 concentration resin, with a median of $3.09 \times 10^{-6}\,\mathrm{S\,cm^{-1}}$ and a max of $3.78 \times 10^{-6}\,\mathrm{S\,cm^{-1}}$; while the 6 wt% Aerosil 380 samples had a median of $1.60 \times 10^{-6}\,\mathrm{S\,cm^{-1}}$ and a max of $3.10 \times 10^{-6}\,\mathrm{S\,cm^{-1}}$. Similarly as in literature [12] we saw a ionic conductivity peak at 4 wt.% Aerosil, these ionic conductivities are a bit lower than the ones found in literature, but our measurements were done in a full device stack obtained from a large area film instead of a small scale no device measurement.

Chapter 5: Conclusions

This thesis investigated the scalable manufacturing of PEG-based solid polymer electrolytes using slot-die coating. We successfully prepared the resin, modified the composition, and slot-die coated relatively homogeneous polymer electrolyte films on graphite electrodes. We were able to optimize the composition, coating, and curing parameters to make a device that achieved good ionic conductivity taking into consideration room temperature measurements, large area film, and full device stack losses. These results show that slot-die coating is a promising scale-up method for PEG-based photocured polymer electrolytes. This work provides a foundation for further scale-up using roll-to-roll for large-scale manufacturing of solid-state batteries.

Chapter 6: Outlook and Future Work

Future work should focus on testing the electrochemical cycling performance of the all-solid-state batteries, investigate other nanofiller chemistry and modifying their concentrations to optimize for slot-die coating. It should also map the topography of the polymer electrolyte to quantitatively measure the homogeneity of the film. Some pre-processing steps show promise on improving the

processability of higher Aerosil concentration resins like using a ball mill to mill the Aerosil before putting it in the resin, but further experiments should quantify how this affects the processability and the ionic conductivity. By having these quantifiable objective metrics, we could further optimize all the variables from Section 3 using a machine learning model[14], and achieve an ideal film for scaling-up. With these coating parameters we could attempt to go into roll-to-roll production and determine the scalability, and repoducibility of this process.

References

[1] Rebecca Bellan. Tracking the EV battery factory construction boom across North America | TechCrunch — techcrunch.com. https://techcrunch.com/2025/02/06/tracking-the-ev-battery-factory-construction-boom-across-north-america/. [Accessed 09-06-2026].

[2] McKinsey Company. Battery 2030: Resilient, sustainable, and circular. https://www.mckinsey.com/industries/automotive-and-assembly/our-insights/battery-2030-resilient-sustainable-and-circular, 2023. [Accessed 12-06-2026].

[3] Peter M. Attia, Eric Moch, and Patrick K. Herring. Challenges and opportunities for high-quality battery production at scale. *Nature Communications*, 16(1), 1 2025.

[4] Wenjia Zhao, Jin Yi, Ping He, and Haoshen Zhou. Solid-state electrolytes for lithium-ion batteries: Fundamentals, challenges and perspectives. *Electrochemical Energy Reviews*, 2(4):574–605, August 2019.

[5] Jun Huang, Chen Li, Dongkai Jiang, Jingyi Gao, Lei Cheng, Guocheng Li, Hang Luo, Zheng-Long Xu, Dong-Myeong Shin, Yanming Wang, Yingying Lu, and Yoonseob Kim. Solid-state electrolytes for lithium metal batteries: State-of-the-art and perspectives. *Advanced Functional Materials*, 35(1), October 2024.

[6] Bengt Sundén. Chapter 4 - battery technologies. In *Hydrogen, Batteries and Fuel Cells*, pages 57–79. Academic Press, 2019.

[7] Jing Ping, Hongbing Pan, PingPing Hou, Meng-Yao Zhang, Xing Wang, Chao Wang, Jitao Chen, Decheng Wu, Zhihao Shen, and Xing-He Fan. Solid polymer electrolytes with excellent high-temperature properties based on brush block copolymers having rigid side chains. *ACS Applied Materials & Interfaces*, 9(7):6130–6137, 2017. PMID: 28128925.

[8] Guang Chen, Shun-Ran Peng, Ying Du, Wei Liu, Zhe Wang, Zong-Bin Lu, Fan Gao, Wei-Qiang Huang, Long-Hai Wang, Chun-Yan Hong, Ze Zhang, and Ye-Zi You. Reshaping li+-polyethylene glycol interactions to boost li+ transport in solid polymer electrolytes. *ACS Applied Materials & Interfaces*, 17(43):59715–59725, 2025. PMID: 41108731.

[9] Ramaswamy I. Venkatanarayanan, Janice L. Lebga-Nebane, Lin Wu, and Sitaraman Krishnan. Lithium coordination and diffusion coefficients of pegylated ionic liquid and lithium salt blends: A molecular dynamics simulation study. *Journal of Molecular Liquids*, 331:115694, 2021.

[10] Jihwan Yoon, Kyengmin Min, Jisoo Song, and Jaewook Nam. Controlling slot-coating edge profiles of battery electrodes. *ACS Applied Materials & Interfaces*, 17(52):70852–70867, 2025. PMID: 41320892.

[11] Prince Aduama, Ameena S. Al Sumaiti, and Khalifa H. Al-Hosani. A multi-perspective review of grid-scale energy storage technologies: Integrating technical, economic, and stakeholder perspectives. *Journal of Energy Storage*, 166:122230, 2026.

[12] Johanna Schwartz, Jayvic Jimenez, Michell Marufu, Micah Silverman, Santiago Tzintzun, Brian Au, Robert Cerda, Chelsea Igtanloc, Katherine Rivadeneira Velasco, Maged Elshatoury, Chloe Lau, Zeyuan Hu, Nishant Ojal, Marissa Wood, Yiran Xiao, Seongkoo Cho, Aldair Gongora, Junhyug Noh, Travis Massey, and Maxwell Marple. Studying-polymers-on a-chip (spoc): High-throughput screening of polymers for battery applications. 3 2025.

[13] Yao Liu, Yang Bai, Wolfram Jaegermann, René Hausbrand, and Bai-Xiang Xu. Impedance modeling of solid-state electrolytes: Influence of the contacted space charge layer. *ACS Applied Materials & Interfaces*, 13(4):5895–5906, 2021. PMID: 33482058.

[14] Ethan Schwartz, Nick Evans, and Daniel Andoue. GitHub - PV-Lab/MOBO-Kit: Multiobjective Bayesian Optimization Toolkit — github.com. `https://github.com/{P}{V}-{L}ab/{M}{O}{B}{O}-{K}it?tab={M}{I}{T}-1-ov-file`. [Accessed 10-06-2026].

[15] Peter Lennartz, Benjamin A. Paren, Abraham Herzog-Arbeitman, Xi Chelsea Chen, Jeremiah A. Johnson, Martin Winter, Yang Shao-Horn, and Gunther Brunklaus. Practical considerations for enabling li|polymer electrolyte batteries. *Joule*, 7(7):1471–1495, 7 2023.

[16] James T. Frith, Matthew J. Lacey, and Ulderico Ulissi. A non-academic perspective on the future of lithium-based batteries. *Nature Communications*, 14(1), 1 2023.

[17] Erin B. Creel, Kristianto Tjiptowidjojo, J. Alex Lee, Kelsey M. Livingston, P. Randall Schunk, Nelson S. Bell, Alexey Serov, and David L. Wood III. Slot-die-coating operability windows for polymer electrolyte membrane fuel cell cathode catalyst layers. *Journal of Colloid and Interface Science*, 610:474–485, 2022.

[18] Andrea Wiegandt, Frederieke Langer, and Julian Schwenzel. Process window evaluation for slot die coating of peo-based electrolytes in all-solid-state batteries. *Energy Technology*, 13(12):2500457, 2025.

[19] Evelina Wikner and Johan Lesser. Accelerated lithium-ion battery cycle lifetime testing by condition-based reference performance tests. *Measurement: Energy*, 4:100019, 12 2024.

[20] Bruis van Vlijmen, Vivek N. Lam, Patrick A. Asinger, Xiao Cui, Joachim Schaeffer, Alexis Geslin, Devi Ganapathi, Shijing Sun, Patrick K. Herring, Chirranjeevi Balaji Gopal, Natalie Geise, Haitao D. Deng, Henry L. Thaman, Stephen Dongmin Kang, Steven B. Torrisi, Amalie Trewartha, Abraham Anapolsky, Brian D. Storey, William E. Gent, Richard D. Braatz, and William C. Chueh. Aging matrix visualizes complexity of battery aging across hundreds of cycling protocols. *Energy & Environmental Science*, 18(13):6641–6654, 2025.

[21] Ruifeng Tan, Weixiang Hong, Jiayue Tang, Xibin Lu, Ruijun Ma, Xiang Zheng, Jia Li, Jiaqiang Huang, and Tong-Yi Zhang. Batterylife: A comprehensive dataset and benchmark for battery life prediction. In *Proceedings of the 31st ACM SIGKDD Conference on Knowledge*

Discovery and Data Mining V.2, KDD '25, pages 5789–5800, New York, NY, USA, 2025. Association for Computing Machinery.

[22] Pooja Vadhva, Ji Hu, Michael J. Johnson, Richard Stocker, Michele Braglia, Dan J. L. Brett, and Alexander J. E. Rettie. Electrochemical impedance spectroscopy for all-solid-state batteries: Theory, methods and future outlook. *ChemElectroChem*, 8(11):1930–1947, May 2021.

[23] Han Cui and Shaofeng Kong. A review on the fabrication and manufacturing processes of all-solid-state batteries from laboratory research to industrial scale-up. *ECS Journal of Solid State Science and Technology*, 15(3):033006, March 2026.